The impact of metallic contacts on propagation losses of an underlying photonic crystal waveguide

The impact of metallic contacts on propagation losses of an underlying photonic crystal waveguide

Peter Kaspar*[a], Roman Kappeler[a], Fouad Karouta[b], Franck Robin[a], Patric Strasser[a], Heinz Jäckel[a]
[a]Electronics Laboratory, ETH Zurich, 8092 Zurich, Switzerland;
[b]COBRA Research Institute, TU Eindhoven, 5612 AZ Eindhoven, Netherlands

ABSTRACT

In view of an electrically pumped photonic crystal-based semiconductor optical amplifier (SOA), we investigate optical mode propagation in 2D PhC waveguides in the presence of metal contacts for carrier injection. Our photonic crystal (PhC) devices are manufactured in the InP/InGaAsP material system. For the loss measurements, we have fabricated contact strips as narrow as 300nm with a sub-50nm placing accuracy on top of W3 waveguides. We study the influence of their position and width on optical power transmission through passive waveguides with respect to viability for future active devices. Our experimental results are complemented by numerical studies (FDTD, plane-wave expansion method).

Keywords: Photonic crystal, W3 waveguide, electrical contact, optical loss, active, SOA, indium phosphide

1. INTRODUCTION

Photonic integrated circuits (PICs) for all-optical signal processing have been investigated for decades. The range of possibilities in this field is enormous, but the compatibility of devices is rather limited. There is no common material system, no common wave-guiding scheme, and a wide variety of fabrication techniques. Coupling between devices is a major challenge for the hybrid integration of functionalities. Non-optimal optical mode matching at waveguide interfaces will lead to losses and reflections, and thus to instabilities and an increased noise level. Therefore, it is interesting to work on a single material system, and to use only one wave-guiding scheme. Such a framework must provide the possibility of monolithic integration of all required functionalities.

For telecom applications, the wavelength of choice is imposed by optical fibers, which are typically operated at a wavelength of 1550nm. Transparency at this wavelength is a prerequisite for a material system to be suitable for communication photonics. Many materials including semiconductors, silica, and polymers are potential candidates that fulfill this requirement. At the forefront of all, silicon is favored due to the extensive availability of process technology from microelectronics. But owing to an indirect electronic bandgap, silicon is unsuitable for active devices. III-V semiconductors like InP and GaAs, on the other hand, offer a direct bandgap, and the fabrication is in many ways similar to silicon technology. Therefore, the III-V semiconductors are found among the top contenders for PICs. InP can be used as a substrate for lattice-matched growth of quaternary InGaAsP layers with a narrower electronic bandgap and a higher refractive index than the substrate. Both active and passive vertical guiding structures can be grown epitaxially by choosing the appropriate quaternary composition.

In microelectronics, performance and cost are improved by reducing the feature size. The limitations are set by lithography. In photonics, however, the effective wavelength of light plays an important role in determining the minimum size of a device. Taking advantage of the photonic bandgap concept of photonic crystals (PhCs)[1], light can be manipulated on a scale of the order of the wavelength λ. Typical lattice constants of hole-type 2D PhC waveguides in InP/InGaAsP heterostructures are around $\lambda/n \approx 500$nm, where $n \approx 3.2$ is the effective refractive index of the vertical guiding structure. Using the slow-light regime of photonic crystals, the group index of refraction can, in theory, become arbitrarily large. This is advantageous for reduced device size (and hence cost) and provides a means for enhancing field strengths and non-linear interaction mechanisms.

In communication photonics, the interplay of several active devices like optical amplifiers, switches, and photodetectors has to be achieved by interconnecting them with passive elements. Ideally, all components are integrated by the same

* kaspar@ife.ee.ethz.ch; phone +41 44 6324022; fax +41 44 6321210; www.photonics.ethz.ch

Active Photonic Crystals II, edited by Sharon M. Weiss, Ganapathi S. Subramania, Florencio García-Santamaría
Proc. of SPIE Vol. 7031, 70310A, (2008) · 0277-786X/08/$18 · doi: 10.1117/12.793687

technology in a modular fashion. An approach using PhCs can potentially satisfy all requirements for such an integration scheme. Coupling losses and reflections at interfaces can be minimized by implementing all functionalities in PhC waveguides. The main challenge, however, is to place electrical contacts onto active components of such a circuit. Very narrow contacts have to be fabricated on a perforated surface. This pushes the process demands to the limits of state-of-the-art semiconductor processing technology.

In planar PhC devices, losses are a major concern. Particularly in substrate-type PhCs, where the refractive index contrast between core and cladding of the vertical guiding structure is small, losses are high[2,3] due to fabrication imperfections. The large vertical mode extension calls for deeply etched holes (~3μm), which can only be attained by compromising on sidewall quality and cylindrical hole shape[4]. For membrane-type PhCs, however, these demands are relaxed, and the optical transmission losses are significantly lower[5,6]. Therefore, passive devices are preferentially implemented in InP membranes, either suspended in air[7,8] or bonded to a low refractive index substrate[9]. For active devices, however, the metal contact introduces additional losses, which are highest when the contact is placed in close proximity to the optical mode. In this respect, the substrate-type PhCs are better suited for active devices.

In this paper, typical substrate-type W3 waveguides (line defects corresponding to three missing rows of holes) for passive applications are investigated with respect to additional losses introduced by metal contacts. The experiment is performed with a relatively thin top cladding of 300nm. This means that, as for membrane-type structures, the optical mode is guided in close proximity of the metal contact. Transmission measurements were performed on waveguides and contact strips of various lengths using the end-fire technique. Loss figures are extracted for access waveguides, plain W3 waveguides and contacted W3 waveguides. In addition, metal losses are estimated using a 1D mode solver and W3 waveguide losses are computed by FDTD.

2. METHODOLOGY

2.1 Fabrication

The starting point of the experiment is a typical PhC waveguide used for passive devices like add-drop filters or power couplers[10]. The optical mode confinement in the vertical dimension is achieved by index guiding in an InP/InGaAsP heterostructure (cf. Fig 3), whereas the lateral confinement arises from the photonic bandgap of the quasi-2D PhC. We chose W3 waveguides instead of W1 to increase manufacturing latitude for the contacts. The hole-type PhCs are fabricated in a three-step lithographic process using an intermediate SiN_x hardmask for dry etching[11]. The nanopattern is written into a 220nm layer of PMMA resist in a 30kV EBL system. Then the structure is transferred into a 30nm layer of Ti and, subsequently, into the 400nm SiN_x hardmask using reactive ion etching (RIE). Finally, the hardmask is used in a Cl_2-based ICP-RIE process to etch the ~3μm deep holes into the semiconductor substrate. A top view SEM analysis of the fabricated holes revealed an average hole diameter of 226nm with a standard deviation of 3.5nm. Given the lattice constant *a* of 380nm, this corresponds to an *r/a* ratio of 0.297. The average was taken over a total of 295 holes.

Deeply etched trench access waveguides for optical transmission measurements are fabricated in the same etching process step as the PhC pattern. To avoid excessive EBL exposure times for the trench waveguides and incoupling tapers, a larger aperture was chosen for their exposure. The dynamic beam placement error between structures written with different apertures was ~300nm (cf. Fig1). This accuracy could be reproduced in the exposure of all fabricated samples.

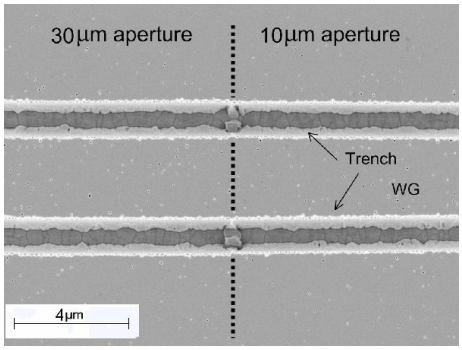

Fig. 1. Interface between trench waveguide sections written with a 10µm and 30µm aperture, respectively. The dynamic beam placement error is <300nm (purely longitudinal in this case).

The metal contact strips are fabricated in a lift-off process using a P(MAA/MMA) resist layer. To guarantee a smooth planarization of the PhC holes, the resist is spin-coated in two steps, resulting in a total layer thickness around 1µm. The contact area is defined by an EBL exposure. The use of a sophisticated marker recognition routine ensured a sub-50nm alignment accuracy of the contact with respect to the PhC structure.

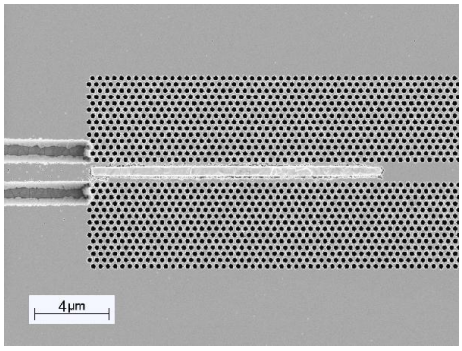

Fig. 2. SEM micrograph of a W3 PhC waveguide with a 15µm long and 300nm wide metal contact strip centered on the waveguide.

2.2 Test structure design

For a complete de-embedding the loss contributions arising from access waveguides, W3 photonic crystal waveguides, and metal contact strips, a set of different waveguide devices was fabricated on a single chip. The schematics of the devices are shown in Fig. 3. They are labeled D1 through D3 from top to bottom. D1 is a pure access waveguide, D2 contains a W3 waveguide of length L, and D3 represents a W3 waveguide of a fixed length L but with a varying contact length l. P_0 is the power coupled into the waveguide and is assumed to be constant for all devices. P_1 through P_3 depict the transmitted power of the devices D1 through D3, respectively. The transmission coefficients at the various interfaces are T_1 through T_5, as shown in Fig. 3. Optical transmission losses are governed by the loss figures attributed to access waveguides (α_A), W3 waveguide devices (α_D), and contacted waveguides (α_C). Of particular interest is the value α_C -α_D, which describes the additional loss caused by the addition of a metal contact strip on top of a passive waveguide.

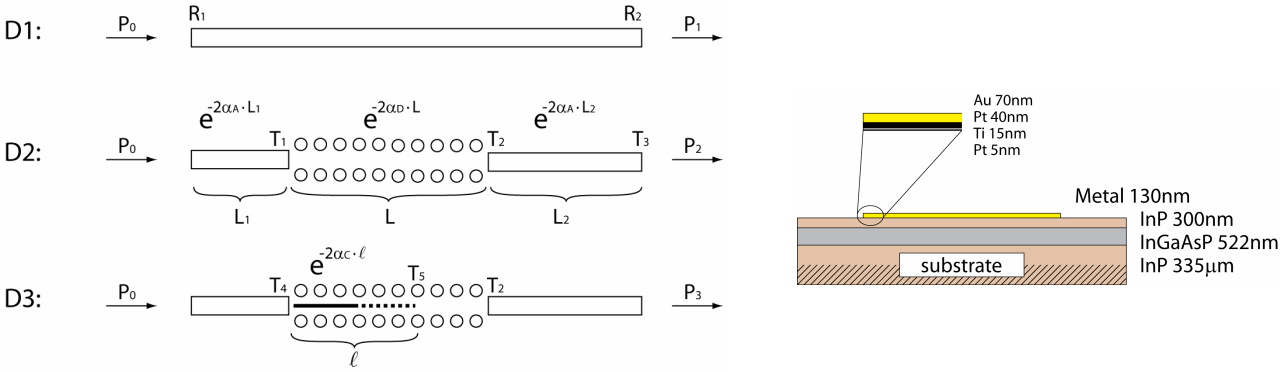

Fig. 3. Left: schematics of the waveguide devices used for the de-embedding of loss contributions arising in access waveguides (D1), W3 photonic crystal waveguides (D2), and metal contact strips (D3). Right: schematic cross-section of the device under test.

For the contact strips, five different configurations were investigated (cf. Fig. 4). Three different widths (300, 500, 1000nm) and, for the narrowest contact, two non-zero lateral offsets from the center position on the W3 waveguide (290, 350nm) were considered.

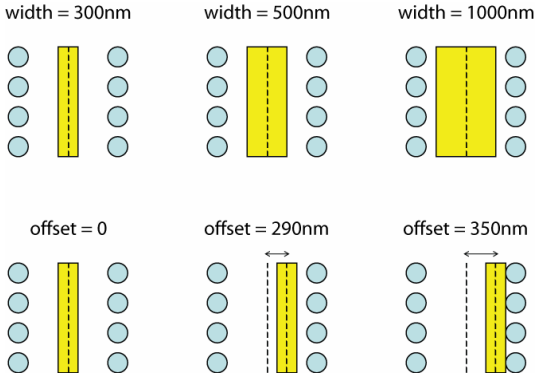

Fig. 4. Contact strip configurations for loss measurements. Three different widths and two non-zero offsets from the center position on the W3 waveguide were designed.

The transmitted powers were measured by the end-fire technique, where the light is coupled into the chip by a lensed fiber and, after propagation through the device, collimated by a microscope objective onto the detector. A 20mW tunable cw laser source was used for wavelength sweeps between 1470nm and 1630nm.

2.3 Loss determination

The losses α_A in our access waveguides are determined by the Fabry-Perot method, also referred to as the Hakki-Paoli method[12] using device D1 of Fig. 3. Fringe patterns are measured with a resolution of 0.005nm and fitted to the transmitted power predicted by Fabry-Perot theory[13]

$$P_1 \sim e^{-2\alpha_A \cdot d} \frac{(1-R_1)(1-R_2)}{(1-e^{-2\alpha_A \cdot d}\sqrt{R_1 R_2})^2 + 4\sqrt{R_1 R_2}\, e^{-2\alpha_A \cdot d} \sin^2(\beta_A)}, \quad (1)$$

where $k_A = \beta_A - i\alpha_A$ is the complex angular wave number of the optical field. For the fit, β_A is fixed using the fundamental frequency of the fringes (from FFT). The total length d of the devices is 3.1mm with an accuracy of 20µm. Furthermore, the reflection coefficients R_1 and R_2 of the cleaved facets are assumed to be equal and are calculated from the effective refractive indices of the semiconductor (determined from the fringe spacing) and air (n =1).

The losses in a W3 waveguide are determined using the cutback method[14]. Output powers of device D2 with W3 waveguides of varying lengths L (15, 30, 60, 120, 240, 480, 960, 1920µm) are measured. With the assumption that the power P_0 coupled into the waveguides is constant for all devices, a linear fit of the measurement data to the relation

$$\ln\left(\frac{P_2(L)}{P_1}\right) = \ln\left(T_1 T_2\right) - 2(\alpha_D - \alpha_A)\cdot L\,, \tag{2}$$

yields the loss figure α_D -α_A, which represents the difference in loss between a PhC waveguide and a trench waveguide. Using the value of α_A determined with the Fabry-Perot method, the PhC waveguide loss α_D can be evaluated.

The additional loss introduced by a metal contact, α_C -α_D, was measured by the same method. Contact strips of varying length l (15, 30, 60, 120, 240µm) were fabricated on top of W3 waveguide devices (D3) of a fixed length (960µm). A linear fit to the function

$$\ln\left(\frac{P_3(l)}{P_2}\right) = \ln\left(\frac{T_4 T_5}{T_1}\right) - 2(\alpha_C - \alpha_D)\cdot l \tag{3}$$

yields the loss figure α_C -α_D. The value of α_C can be retrieved by subtracting α_D from the W3 waveguide measurement. This constitutes a full de-embedding of loss contributions into access waveguide, PhC waveguide and contact.

3. RESULTS

3.1 Access waveguide losses

The losses of the deep trench waveguides, were extracted from Fabry-Perot fringes. Fig. 5 shows a typical measurement at λ =1550nm (dotted blue) and the fitted curve (solid red) according to Eq. 1. A loss figure of α_A = 2.565cm^{-1} is extracted for the 3µm wide trench waveguide. This corresponds to 22.3dB/cm.

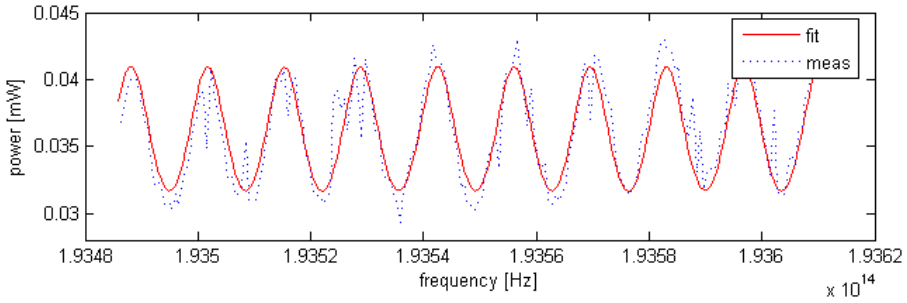

Fig. 5. Fabry-Perot fringes at λ =1550nm of a 3.1cm long cavity formed by a 3µm wide trench waveguide between two cleaved facets. The transmitted power [mW] is plotted against frequency [Hz]. The dotted blue line is the measurement, the solid red line is a fit according to the model of Eq. 1.

3.2 W3 waveguide losses

Using Eq. 2, the loss figures α_D -α_A of the W3 waveguides were retrieved from the ratios of output powers $P_2(L)/P_1$. Fig. 6 shows the losses as a function of wavelength, including statistical error bars (95% confidence intervals) from the fitting procedure. The increase in size of the confidence intervals towards the edges of the laser spectrum can be explained by the decrease in laser power and stability.

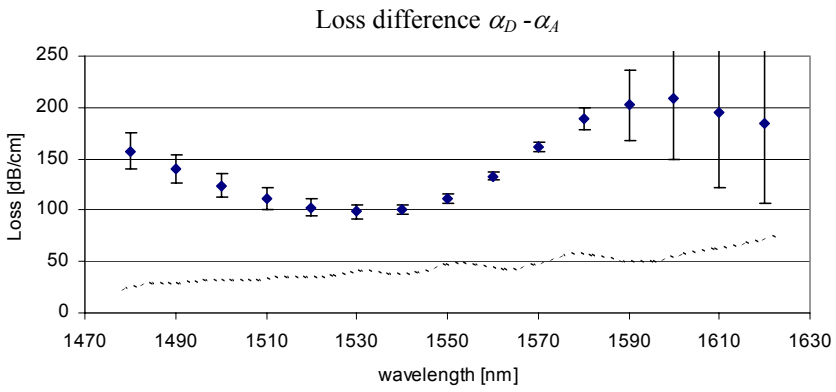

Fig. 6. Transmission loss difference between a W3 PhC waveguide and a trench access waveguide. The error bars represent the 95% confidence intervals of the exponential fits to the measurement data. The dashed line represents the simulated FDTD loss spectrum as shown in Fig. 7-a.

Adding the access waveguide loss of 22.3dB/cm at λ =1550nm, we obtain a W3 loss figure of 133.5dB/cm. This corresponds to the state-of-the-art for reactive ion etching (RIE) technology[3]. Better results, around 20dB/cm, were obtained using chemically assisted ion-beam etching (CAIBE)[2].

Using 3D FDTD simulations[15], the transmission spectrum was calculated for a W3 slab waveguide, surrounded by perfectly matched layers (PML). The transmission was determined as the ratio of intensity fluxes measured for two detectors as depicted in Fig 7. The first detector is separated from the source by 6.5 lattice periods to ensure mode settling. Simulations were performed for various resolutions up to 30 grid points per period using epsilon averaging[15]. The solutions are well converged. The results show that, within the spectral window covered by the laser source, the loss profile is rather flat (cf. Fig. 7). Our measurements are situated between the lower bandgap edge at λ =1730nm and a pronounced peak around λ =1440nm. We attribute this peak to a mini stop band as indicated in Fig. 8. An average loss of 44dB/cm is computed for a W3 waveguide. The average is used as a first estimate for comparison with our measurements and is taken over the entire laser tuning frequency range. The computed loss is considerably lower than the measured one. We attribute this to fabrication imperfections of the real devices, such as conical hole shape, surface roughness as well as hole placement disorder.

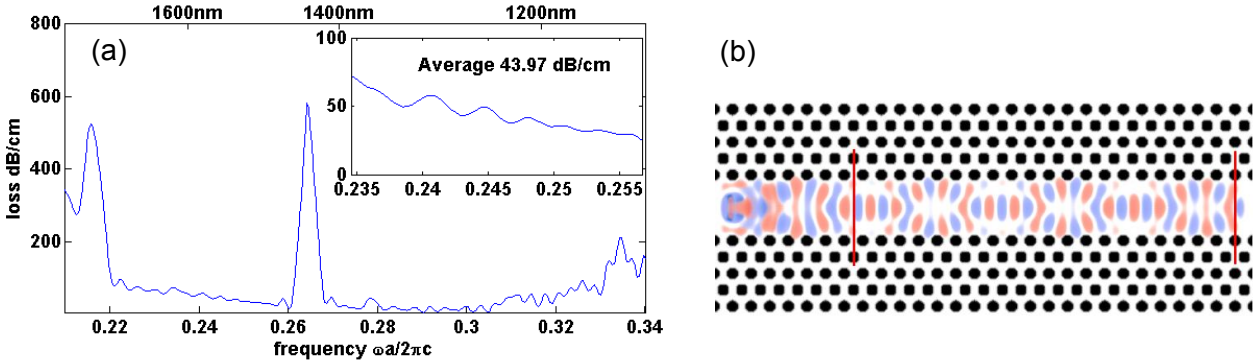

Fig. 7. FDTD loss spectrum of our W3 waveguide (a). Losses are plotted versus reduced frequency $\omega a/2\pi c = a/\lambda$. The inset shows the spectral range used for the measurements presented in Fig. 6. The computed loss (a) is measured between the detectors indicated by two vertical lines in the 2D representation of the 3D FDTD model (b). The magnetic field pattern is shown for a continuous excitation at λ =1550nm.

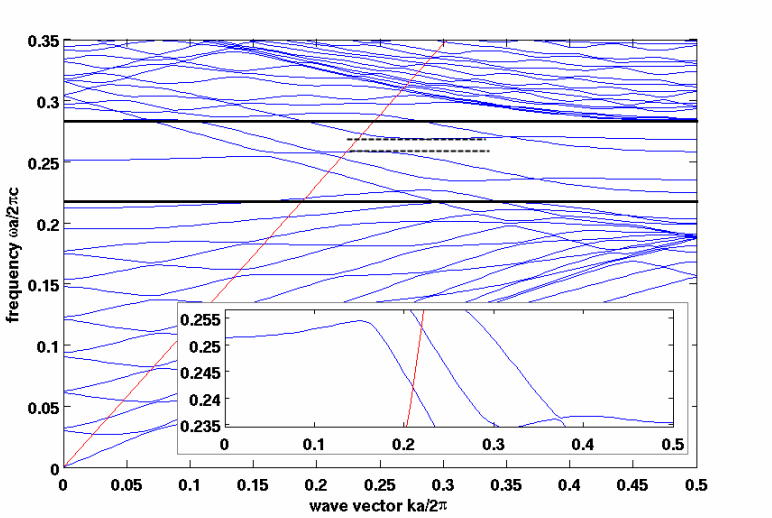

Fig. 8. Band diagram of a W3 PhC waveguide with a lattice constant a =380nm and an r/a ratio of 0.297, computed by MPB[16]. Reduced frequency $\omega a/2\pi c = a/\lambda$ is plotted against the angular wavenumber k in units of $2\pi/a$. The solid horizontal lines indicate the boundaries of the PhC bandgap. The light cone in air is represented by a red line. The inset shows a close-up view of the frequency range covered by the measurements. The loss peak around λ =1440nm in Fig. 7 is attributed to the mini stop band indicated by the dashed lines.

3.3 Contact losses

The loss parameters for the contacts on W3 waveguides were extracted from a linear fit according to Eq. 3. The coefficients of determination, R^2, of the linear fits at a wavelength of 1550nm are all greater than 0.94, except for the contact width of 500nm, where we only got 0.83.

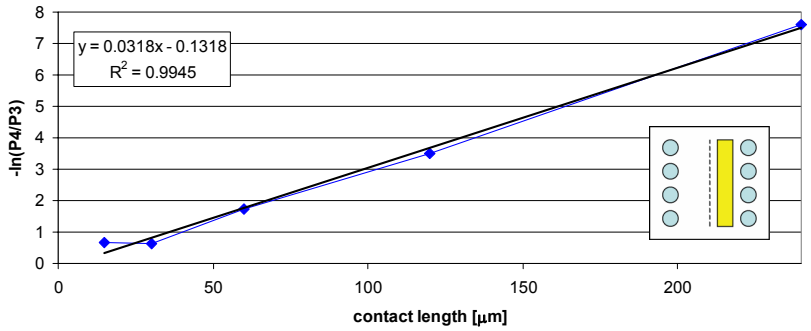

Fig. 9. Example of a linear fit to the measurement data of a contacted W3 PhC waveguide. The inset shows the contact configuration: 300nm wide contact with a 290nm offset from its center position on the waveguide

Fig. 9 shows the example of a 300nm wide contact strip with an offset of 290nm from the waveguide's center position, measured at a wavelength of 1550nm. The resulting loss figure is 1350±100dB/cm. Fig. 10 shows all loss numbers α_C - α_D measured for the different contact configurations of Fig. 4.

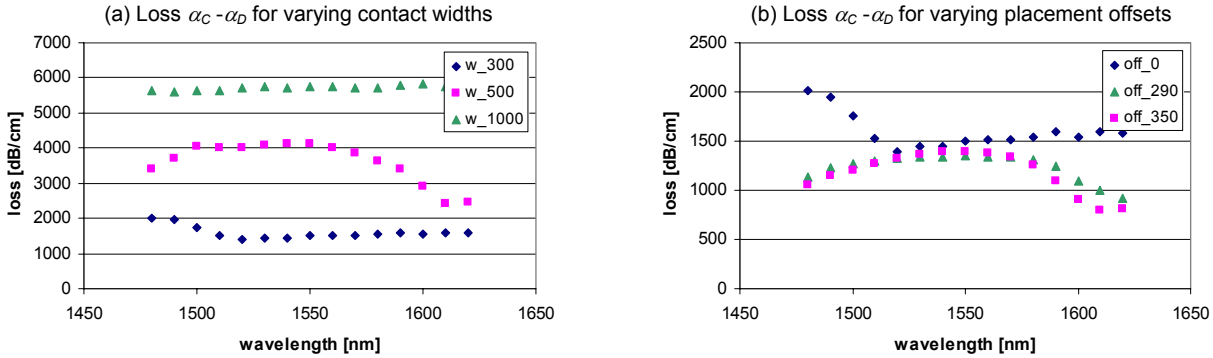

Fig. 10. Loss numbers α_C -α_D versus wavelength measured between 1480nm and 1620nm. Contacts of varying width (300, 500, 1000nm), positioned at the center of the waveguide (left) are shown as well as contacts of a fixed width of 300nm with a varying offset (0, 290, 350nm) from the center position (right).

The additional loss introduced by the metal contact strip is very high (>1000dB/cm) and increases with contact width (Fig. 10-a). For the narrowest contacts fabricated (300nm), the metal strips will add ten times the dB-loss of the W3 waveguide. The widest contact fabricated is 1000nm, which corresponds to almost the full width of the waveguide (1090nm). It shows four times the dB-loss of the narrower 300nm contacts.

The lateral positioning of the contact on the waveguide, on the other hand, doesn't reveal any clear trends (Fig. 10-b). This can be attributed to the fact that our W3 waveguides are multi-mode and that our contacts are too wide to resolve the variations in field intensitiy of the modes (cf. Fig.7-b). For single-mode operation, a maximum loss would be expected for the center position of the contact, because in that case the strongest field intensities would coincide with the contact position. However, for single-mode operation, the width of the waveguide (~430nm for W1) would be of the same order as the narrowest of our contact strips. The resulting placement latitude would be too small for a similar experiment on single-mode waveguides.

For an electrically pumped PhC SOA, the propagation losses have to be minimized. This can be achieved by narrowing the metal contacts or by increasing the thickness of the top cladding of the vertical guiding structure. The fabrication of contacts narrower than 300nm is challenging due to the planarization issue of the perforated PhC device surface. For the purpose of the presented experiment, the top cladding thickness is intentionally chosen to be only 300nm, which means that the optical mode is significantly exposed to the metal contact. Fig. 12 shows the losses versus top cladding thickness, computed with a 1D mode solver. Losses are estimated using the complex refractive index $n+i\kappa$ of gold, where n =0.559 and κ =9.81 at λ =1550nm[17]. The agreement with our measurement for the 1000nm wide contact is remarkable. Since the simulation is 1D, it corresponds best to the experimental situation with the widest contact. To decrease the contact losses to a level comparable to the W3 waveguide losses, the top cladding thickness has to be increased to ~1μm.

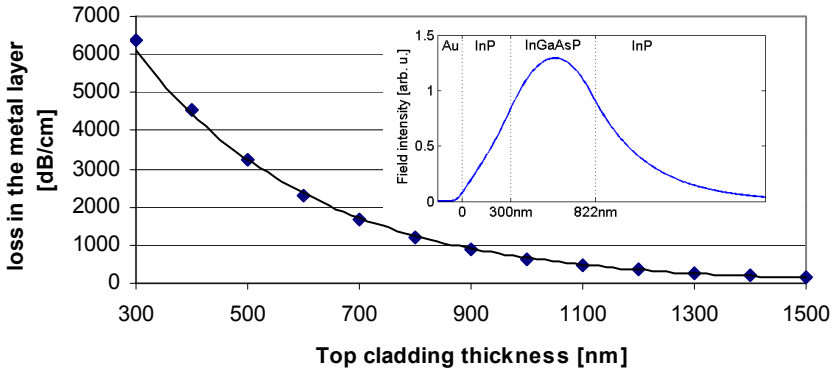

Fig. 11. 1D simulation of contact loss versus top cladding thickness of the vertical guiding structure. The solid line is an exponential fit to the calculated points. The inset shows an intensity profile of the mode corresponding to a 300nm top cladding; intensity is plotted against InP/InGaAsP/InP depth (the origin is set at the semiconductor surface).

A thicker top cladding (~1μm) pushes the optical mode deeper below the device surface, which, in turn, raises the demand for deeper (~4μm) PhC holes in order to ensure lateral bandgap guiding. There is a trade-off between contact losses and the losses arising from imperfect PhC fabrication. This trade-off has to be optimized for the development of efficient active devices.

4. CONCLUSION

Loss measurements of contacted W3 PhC waveguides have been presented. A full de-embedding of loss contributions of access trench waveguides, W3 PhC waveguides and metal contact strips has been successfully achieved. W3 waveguide losses of 133.5dB/cm are comparable to state-of-the-art. The additional losses of >1500dB/cm introduced by the metal contact strip are very high. For the 1000nm wide contacts, covering almost the full width of the W3 waveguides, losses of ~6000dB/cm are measured, which is in good agreement with our predictions (1D mode solver). The high loss values can be explained by the small thickness of 300nm of the top cladding, which was chosen thinner than for a typical active device. A thickness of ~1μm is required to reduce the losses to a level comparable to W3 waveguide losses. This affirms that electrically pumped active membrane-type PhC devices are out of reach for state-of-the-art nanofabrication technology. For substrate-type active devices, a balance between large mode overlap with the contact layers and lossy waveguides due to reduced PhC hole quality (deeply etched holes) has to be found.

ACKNOWLEDEMENT

The authors would like to express their gratitude to Prof. J. Faist from the quantum electronics group of ETH Zurich who is the author of the particular 1D mode solver used for this work.

REFERENCES

[1] Joannopoulos, J. D., Johnson, S. G., Winn, J. N. and Meade, R. D., [Photonic Crystals: Molding the Flow of Light (second edition)], Priceton University Press, Princeton and Oxford, (2008).

[2] Kotlyar, M. V., Karle, T., Settle, M. D., O'Faolain, L. and Krauss, T. F., "Low-loss photonic crystal defect waveguides in InP," Appl. Phys. Lett. 84(18), 3588-3590 (2004).

[3] Talneau, A., Le Gouezigou, L. and Bouadma, N., "Quantitative measurement of low propagation losses at 1.55 μm on planar photonic crystal waveguides," Opt. Lett. 26(16), 1259-1261 (2001).

[4] Strasser, P., Wüest, R., Robin, F., Erni, D. and Jäckel, H., "Detailed analysis of the influence of an inductively coupled plasma reactive-ion etching process on the hole depth and shape of photonic crystals in InP/InGaAsP," J. Vac. Sci. Technol. B 25(2), 387-393 (2007).

[5] Gerace, D. and Andreani, L., "Low-loss guided modes in photonic crystal waveguides,"Opt. Express 13(13), 4939-4951 (2005).
[6] Tanaka, Y., Sugimoto, Y., Ikeda, N., Nakamura, H., Asakawa, K., Inoue, K. and Johnson, S.G., "Group velocity dependence of propagation losses in single-line-defect photonic crystal waveguides on GaAs membranes," Electron. Lett. 40(3), 174-176 (2004).
[7] Sugimoto, Y., Tanaka, Y., Ikeda, N., Nakamura, Y., Asakawa, K. and Inoue K., "Low propagation loss of 0.76 dB/mm in GaAs-based single-line-defect two-dimensional photonic crystal slab waveguides up to 1 cm in length," Opt. Express 12(6), 1090-1096 (2004).
[8] Scherer, A., Painter, O., D'Urso, B., Lee, R. and Yariv A., "InGaAsP photonic band gap crystal membrane microresonators," J. Vac. Sci. Technol. B 16(6), 3906-3910 (1998).
[9] Saitoh, T., Sogawa, T., Notomi, M., Tamamura, T., Kodama, S., Furuta, T. and Ando, H., "GaAs photonic crystals on SiO_2 fabricated by very-high-frequency anode-coupled reactive ion etching and wafer bonding," Jpn. J. Appl. Phys. 39, 6259-6263 (2000).
[10] Strasser, P., Flückiger, R., Wüest, R., Robin, F. and Jäckel, H., "InP-based compact photonic crystal directional coupler with large operation range," Opt. Express 15(13), 8472-8478 (2007).
[11] Wüest, R., Strasser, P., Robin, F., Erni, D. and Jäckel, H., "Fabrication of a hard mask for InP based photonic crystals: Increasing the plasma-etch selectivity of poly(methyl methacrylate) versus SiO_2 and SiN_x," J. Vac. Sci. Technol. B 23(6), 3197-3201 (2005).
[12] Hakki, B. W. and Paoli, T. L., "CW degradation at 300 degrees K of GaAs double heterostructure junction lasers. II. electronic gain," J. Appl. Phys., 44(9), 4113–4119 (1973).
[13] Saleh, B. E. A. and Teich, M. C., [Fundamentals of Photonics], Wiley, New York, Chap. 7.1 (2007).
[14] Notomi, M., Shinya, A., Yamada, K., Takahashi, J.-I., Takahashi, C. and Yokohama, I., "Structural tuning of guiding modes of line-defect waveguides of silicon-on-insulator photonic crystal slabs," IEEE J. Quantum Electron. 38(7), 736–742 (2002).
[15] Farjadpour, A., Roundy, D., Rodriguez, A., Ibanescu, M., Bermel, P., Joannopoulos, J. D., Johnson, S. G. and Burr, G., "Improving accuracy by subpixel smoothing in FDTD," Opt. Lett. 31(20), 2972–2974 (2006).
[16] Johnson, S. G and Joannopoulos, J. D., "Block-iterative frequency-domain methods for Maxwell's equations in a planewave basis," Opt. Express 8(3), 173-190 (2001).
[17] Palik, E. D., [Handbook of Optical Constants of Solids I], Academic Press, 286-295 (1985).